Journal of Materials Chemistry A

COMMUNICATION

View Article Online
View Journal | View Issue

Cite this: J. Mater. Chem. A, 2018, 6, 18847

Received 29th July 2018
Accepted 6th September 2018

DOI: 10.1039/c8ta07334a

rsc.li/materials-a

Extension of indacenodithiophene backbone conjugation enables efficient asymmetric A–D–A type non-fullerene acceptors†

Jiali Song,‡[a] Chao Li,‡[a] Linglong Ye,[a] Changwoo Koh,[b] Yunhao Cai,[a] Donghui Wei,[c] Han Young Woo[b] and Yanming Sun*[a]

A novel strategy involving judiciously fusing one thiophene/thieno[3,2-*b*]thiophene on only one side of an indacenodithiophene (IDT) unit to extend IDT backbone conjugation was developed, and three A–D–A type non-fullerene small molecules (**TPT-2F**, **TPTT-2F**, and **TPTTT-2F**) were designed and synthesized to investigate the influence of the extent of IDT core conjugation on their photovoltaic properties. Extending the IDT core conjugation could broaden absorption, upshift the lowest unoccupied molecular orbital (LUMO) energy level, enhance electron mobility, and increase intermolecular π–π stacking. When these three non-fullerene acceptors were applied in organic solar cells (OSCs), simultaneous enhancement of the open-circuit voltage (V_{oc}), short-circuit current (J_{sc}), and fill factor (FF) was obtained, with the degree of enhancement following the order **TPT-2F** < **TPTT-2F** < **TPTTT-2F**. As a result, the **TPTTT-2F** based OSCs yielded a high PCE of 12.03%. To the best of our knowledge, the PCE of 12.03% is among the highest values for asymmetric non-fullerene acceptor based OSCs so far. These results demonstrate that extending the conjugation of the IDT core is an effective approach to design highly efficient asymmetric non-fullerene acceptors.

Introduction

Organic solar cells (OSCs) have aroused considerable research interest among the academic and industrial communities, owing to their distinctive advantages of low cost, light weight, mechanical flexibility, and solution processability.[1] Generally, the photoactive layers of OSCs are fabricated with a bulk heterojunction structure composed of a polymer donor and an n-type semiconductor acceptor. In the past few decades, fullerene derivatives played a dominant role as n-type semiconductor acceptors, due to their high electron mobility and superior isotropic charge transporting abilities.[2,3] However, they suffer from several inherent shortcomings, including high production cost, weak absorption in the visible region, and limited molecular energy level tunability, which restrict their further applications in OSCs.[4] On the other hand, non-fullerene acceptors (NFAs) have emerged as a promising alternative to replace fullerene derivatives in the last few years,[5–8] and significant advancements in non-fullerene-based OSCs have been achieved, with power conversion efficiencies (PCEs) reaching 14%.[9] In the design and synthesis of non-fullerene acceptors, an acceptor–donor–acceptor (A–D–A) backbone architecture is thought to be beneficial for enhancing the intramolecular charge transfer (ICT).[10–15] In such A–D–A type NFAs, the D and A are a fused-ring electron donating core unit and an electron accepting terminal unit, respectively. Through rational chemical modification and proper selection of the D and/or A unit, the absorption spectra, molecular energy levels, push–pull effect, and intermolecular interactions of the resultant NFAs can be fine-tuned.[7]

For the A unit, 1,1-dicyanomethylene-3-indanone (IC) has become one of the most widely used end-capping groups in the design of efficient NFAs.[12,16,17] Monofluorination of the IC end-capping group is a simple approach to further enhance the ICT effect without significantly decreasing the open-circuit voltage (V_{oc}).[18] Additionally, introducing one fluorine atom onto the IC end-capping group is also advantageous for enhancing the charge transporting abilities of the resultant NFAs, which could be partly ascribed to the formation of C–F···H, C–F···S, and C–F···π noncovalent interactions.[19] Accordingly, these promising properties of monofluorinated IC end-capping groups have proved to be effective in designing highly efficient NFAs.[11,20,21]

For the D unit, the use of the five-membered indacenodithiophene (IDT) moiety has become a popular approach to designing A–D–A type NFAs.[22,23] To further tune the ICT effect for a given A unit, several methods have been adopted to modify

[a]School of Chemistry, Beihang University, Beijing 100191, China. E-mail: sunym@buaa.edu.cn

[b]Department of Chemistry, College of Science, Korea University, Seoul 136-713, Republic of Korea

[c]The College of Chemistry and Molecular Engineering, Zhengzhou University, Zhengzhou, Henan Province 450001, China

† Electronic supplementary information (ESI) available. See DOI: 10.1039/c8ta07334a

‡ These two authors contributed equally to this work.

the chemical structure of the IDT core unit, such as core conjugation regulation,[12,24,25] heteroatom substitution,[26] side chain engineering,[27–31] and π-spacer modulation,[32–36] among others. In particular, the modulation of IDT core conjugation has effectively promoted the development of NFAs.[9,12,25] For example, Zhan *et al.* reported a symmetric star-shaped compound ITIC, in which one thiophene is fused to each side of the five-membered central core IDT unit.[12] By fusing one thieno[3,2-*b*]thiophene on each side of the IDT unit, the same group reported a new nine-membered IDT derivative referred to as the symmetric IBDT unit, and designed a corresponding high-performance non-fullerene acceptor INIC3 with an outstanding PCE of 11.5%.[25]

Modulation of the core conjugation *via* fusing one thiophene or thieno[3,2-*b*]thiophene on each side of the five-membered IDT unit generally leads to symmetric IDT derivatives. However, very limited attempts have been devoted toward fusing a thiophene or thieno[3,2-*b*]thiophene to only one side of an IDT unit, which could be partly ascribed to challenging synthesis and purification of such compounds.[16,37,38] Intriguingly, different from the approach of fusing one thiophene or thieno[3,2-*b*]thiophene to each side of the IDT unit, the strategy of fusing a thiophene or thieno[3,2-*b*]thiophene on only one side of the IDT unit could result in novel asymmetric IDT derivatives, which would provide a new method to adjust the conjugation of the symmetric IDT core. Moreover, there is very limited research on the influence of different extents of IDT core conjugation on the photovoltaic performance of the corresponding asymmetric A–D–A type NFAs (Fig. 1).[39–41]

Very recently, we have reported a novel asymmetric TPTT unit, which integrates thiophene (T), phenylene (P), and thieno[3,2-*b*]thiophene (TT) units into a single fused molecular entity.[16] This molecular configuration not only makes the TPTT unit asymmetric, but also extends the conjugation length of TPTT compared to the IDT unit. In order to further extend the backbone conjugation, in this contribution, we designed and synthesized a novel IDT derivative, **TPTTT**, in which thiophene (T), phenylene (P), and dithieno[3,2-*b*:2′,3′-*d*]thiophene (TTT) segments are condensed with two embedded cyclopentadienyl moieties. From the five-membered IDT unit to the six-membered TPTT unit and seven-membered **TPTTT** unit, the backbone conjugation, π-electron delocalization and electron donating ability would be progressively extended. It was expected that the ICT between the central core unit and the terminal accepting unit would also be enhanced sequentially when these three units were applied in A–D–A type NFAs.

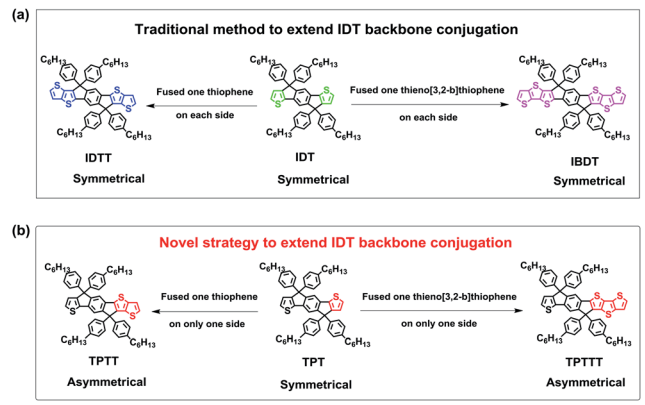

Fig. 1 (a) Traditional method to extend IDT backbone conjugation; (b) novel strategy to extend IDT backbone conjugation.

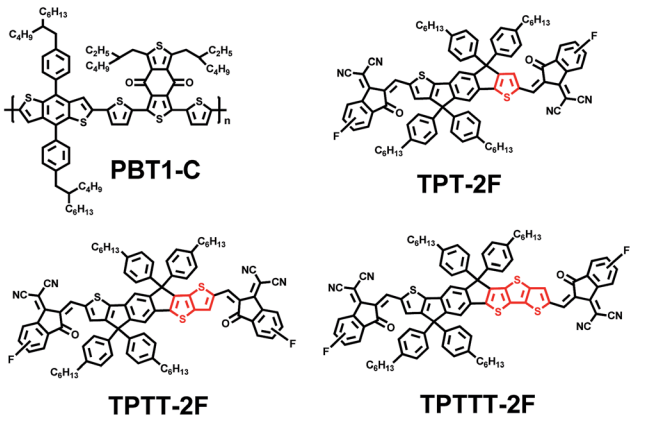

Fig. 2 Chemical structures of PBT1-C, TPT-2F, TPTT-2F, and TPTTT-2F.

In this work, to take advantage of the monofluorination of the IC end-capping group and investigate the impact of different IDT backbone conjugation lengths on the photovoltaic properties of NFAs, the TPT, TPTT, and **TPTTT** units are used as the central electron donating core unit in conjunction with a monofluorinated IC end-capping group as the terminal electron accepting unit. The symmetric NFA **TPT-2F** and the asymmetric NFAs **TPTT-2F** and **TPTTT-2F** were synthesized (Fig. 2), and the red shift of the absorption spectrum, LUMO energy level, and electron mobility were found to follow the order **TPT-2F** < **TPTT-2F** < **TPTTT-2F**. As a result, the OSCs based on **PBT1-C** : **TPTTT-2F** delivered a maximum PCE of 12.03% with an open-circuit (V_{oc}) of 0.916 V, a short-circuit current (J_{sc}) of 17.63 mA cm^{-2}, and a fill factor (FF) of 0.745, which were superior to the performance of the **PBT1-C** : **TPT-2F** and **PBT1-C** : **TPTT-2F** devices. To the best of our knowledge, the PCE of 12.03% is among highest values for asymmetric non-fullerene acceptor based OSCs at present.[16,37,38,42] These results demonstrate that extending the IDT core conjugation is an effective way to design highly efficient asymmetric non-fullerene acceptors. More importantly, extending the IDT core conjugation length in A–D–A type nonfullerene acceptors enables simultaneous increases in V_{oc}, J_{sc}, and FF, thus resulting in high PCEs.

Results and discussion

The syntheses of **TPT-2F**, **TPTT-2F**, and **TPTTT-2F** are shown in Scheme 1. Firstly, compound **1** was reacted with tributyl(dithieno[3,2-*b*:2′,3′-*d*]thiophen-2-yl)stannane *via* the Stille coupling reaction to produce compound **2**. Then, the treatment of compound **2** with (4-hexylphenyl)lithium afforded two benzyl alcohols, followed by a ring-closure reaction by treatment with BF_3 etherate to yield the novel asymmetric building block

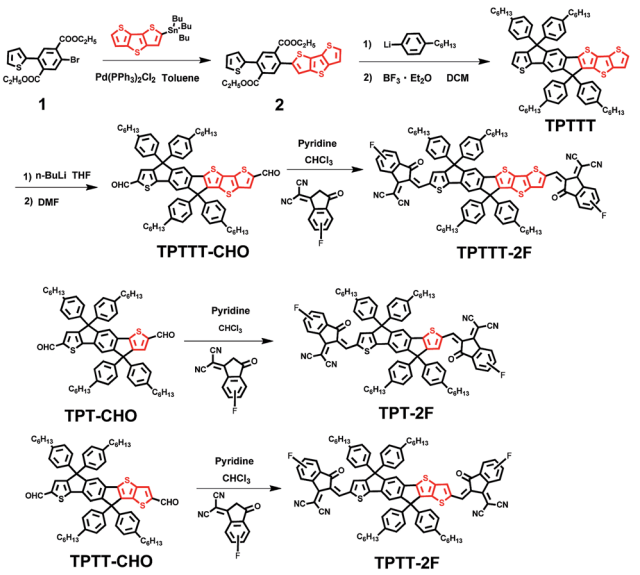

Scheme 1 Synthetic routes of TPT-2F, TPTT-2F, and TPTTT-2F.

TPTTT. Afterwards, **TPTTT** was reacted with *n*-butyllithium followed by treatment with dry DMF to afford **TPTTT-CHO**. Finally, the Knoevenagel condensation reaction of the monofluorinated IC end-capping group with **TPT-CHO**, **TPTT-CHO**, or **TPTTT-CHO** yielded non-fullerene small molecules **TPT-2F**, **TPTT-2F**, and **TPTTT-2F**, respectively. All the intermediates and the three non-fullerene small molecules were thoroughly characterized using ^{1}H NMR, ^{13}C NMR, and HRMS (ESI†). In addition, these three non-fullerene small molecules could be readily dissolved in common organic solvents, such as dichloromethane, tetrahydrofuran, and chlorobenzene.

The normalized absorption spectra of the three NFAs in dilute chloroform solution and thin films are shown in Fig. 3, and the related data are presented in Table 1. In dilute chloroform solution, maximum absorption peaks located at 662, 675, and 687 nm were observed for **TPT-2F**, **TPTT-2F**, and **TPTTT-2F**, respectively, along with a prominent shoulder peak for each NFA. The thin film of each NFA exhibited a broader absorption spectrum and a red-shifted absorption maximum relative to the corresponding solution. Specifically, the absorption maxima of **TPT-2F**, **TPTT-2F**, and **TPTTT-2F** were red-shifted from 662 to 698 nm, from 675 to 717 nm, and from 687 to 724 nm, respectively, suggesting strong intermolecular interactions among these three NFAs in the solid state. The absorption onsets of the **TPT-2F**, **TPTT-2F**, and **TPTTT-2F** thin films were located at 754, 785, and 794 nm, which corresponded to optical bandgaps (E_g^{opt}) of 1.64, 1.58, and 1.56 eV, respectively. The progressive red shift in the absorption spectra and narrowing of the bandgap from symmetrical **TPT-2F** to asymmetric **TPTT-2F** and **TPTTT-2F** could be ascribed to the extended IDT core conjugation and stronger electron-donating ability.[43]

The frontier molecular orbitals and corresponding energy levels of the three NFAs, which were calculated using the density functional theory (DFT) method at the B3LYP/6-31G(d, p) level, are depicted in Fig. S1.† For all three NFAs, the electron density of the HOMO was mainly localized on the central electron-donating unit, while the electron density of the LUMO was well distributed over both the central core unit and the terminal monofluorinated IC end-capping group. The calculated HOMO/LUMO energy levels of **TPT-2F**, **TPTT-2F**, and **TPTTT-2F** were −5.74/−3.51 eV, −5.64/−3.47 eV, and −5.57/−3.44 eV, respectively, suggesting that extending the IDT core conjugation upshifted both the HOMO and LUMO energy levels.

The electrochemical properties of the three NFAs were evaluated by cyclic voltammetry measurements. As shown in Fig. 3c, the onset oxidation/reduction potentials of **TPT-2F**, **TPTT-2F**, and **TPTTT-2F** were measured to be 1.47/−0.31, 1.38/−0.33 and 1.33/−0.36 V, respectively. From these potentials, the HOMO/LUMO energy levels of **TPT-2F**, **TPTT-2F**, and **TPTTT-2F** were determined to be −5.84/−4.06, −5.75/−4.04 and −5.70/−4.01 eV, respectively. These results indicated that extending the IDT core conjugation upshifted both HOMO and LUMO energy levels, which was in good agreement with the results of the DFT calculation. In addition, the shifts in the HOMO energy levels were more pronounced than those of the LUMO energy levels.[39] It is worth noting that, due to the longer core conjugation length and stronger electron-donating ability of **TPTTT** compared to those of TPT and TPTT, **TPTTT-2F** exhibited a higher LUMO energy level relative to the other two NFAs, which would be beneficial for obtaining a higher V_{oc} in OSCs.

To evaluate the photovoltaic performance of the three NFAs, we chose **PBT1-C**, which was recently reported by our group,[44] as the donor to fabricate bulk heterojunction (BHJ) OSCs with an inverted device structure of ITO/ZnO/**PBT1-C** : NFA/MoO_3/Ag. We carefully investigated the device processing conditions, including the donor/acceptor (D/A) weight ratio and the content of the additive 1,8-diiodooctane (DIO), to obtain the best photovoltaic performance. The optimal D/A weight ratio and DIO content were found to be 1 : 1 and 0.25%, respectively. The resulting **PBT1-C** : **TPTTT-2F** device delivered an optimal PCE of 12.03% with a V_{oc} of 0.916 V, a J_{sc} of 17.63 mA cm^{-2}, and a FF of 0.745. These values were superior to the optimal PCE of 8.33%, V_{oc} of 0.874 V, J_{sc} of 13.89 mA cm^{-2}, and FF of 0.686 for the

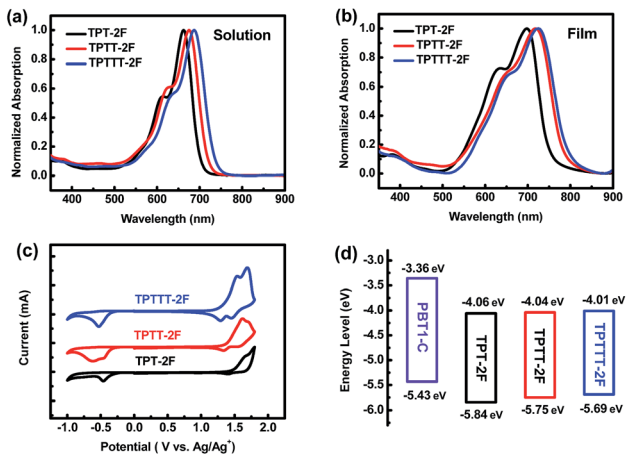

Fig. 3 (a) Absorption spectra of the three NFAs in chloroform solution and (b) in thin films; (c) cyclic voltammograms of the three NFAs; (d) energy level diagram of PBT1-C and the three NFAs.

Table 1 Optical and electrochemical properties of the three NFAs

NFA	λ_{max}[a] [nm]	λ_{max}[b] [nm]	λ_{onset}[b] [nm]	E_g^{optc} [eV]	E_{ox} [V]	HOMO [eV]	E_{red} [V]	LUMO [eV]
TPT-2F	662	698	754	1.64	1.47	−5.84	−0.31	−4.06
TPTT-2F	675	717	785	1.58	1.38	−5.75	−0.33	−4.04
TPTTT-2F	687	724	794	1.56	1.32	−5.69	−0.36	−4.01

[a] In $CHCl_3$ solution. [b] In a thin film drop cast from the $CHCl_3$ solution. [c] Estimated from the empirical formula: $E_g^{opt} = 1240/\lambda_{onset}$.

PBT1-C : TPT-2F device, and to the optimal PCE of 10.17%, V_{oc} of 0.881 V, J_{sc} of 15.82 mA cm^{-2}, and FF of 0.73 for the **PBT1-C : TPTT-2F** device. Moreover, the optimized **PBT1-C : TPTTT-2F** device exhibited an energy loss of 0.644 eV, which was lower than the energy loss of 0.766 eV for the optimized **PBT1-C : TPT-2F** device and 0.699 eV for the optimized **PBT1-C : TPTT-2F** device. These results demonstrated that the **TPTTT-2F** based device with more extended IDT core conjugation not only exhibited a lower energy loss, but also simultaneously achieved a higher V_{oc}, higher J_{sc}, and higher FF, thus leading to a higher PCE. The *J*–*V* curves and corresponding photovoltaic data of the optimized device are provided in Fig. 4a and Table 2, respectively.

The external quantum efficiency (EQE) curves of the optimized devices are displayed in Fig. 4b. From the **PBT1-C : TPT-2F** to the **PBT1-C : TPTT-2F** and **PBT1-C : TPTTT-2F** devices, the maximum EQE value gradually increased, and the photoresponse was extended to longer wavelengths. As a result, the **PBT1-C : TPTTT-2F** device exhibited a high integrated J_{sc} of 16.88 mA cm^{-2}, which was higher than the J_{sc} values of 13.41 mA cm^{-2} for the **PBT1-C : TPT-2F** device and 15.23 mA cm^{-2} for the **PBT1-C : TPTT-2F** device. These results indicated that the **TPTTT-2F** based device with the most extended conjugation showed more efficient photon harvesting and charge collection efficiency. Moreover, these integrated J_{sc} values agreed well with the J_{sc} values obtained from *J*–*V* curves, within 5% mismatch.

The charge transport properties of the three NFA films and the corresponding blend films were investigated *via* space charge limited current (SCLC) measurement. The average electron mobilities of the neat **TPT-2F**, **TPTT-2F**, and **TPTTT-2F** films were measured to be 4.17 × 10^{-4}, 4.53 × 10^{-4}, and 4.82 × 10^{-4} cm^2 V^{-1} s^{-1}, respectively. These results demonstrated that extending the IDT core conjugation in NFAs enhanced the electron mobility. After blending with **PBT1-C**, the average hole/electron mobilities of the **PBT1-C : TPT-2F**, **PBT1-C : TPTT-2F**, and **PBT1-C : TPTTT-2F** devices were determined to be 3.51 × 10^{-4}/0.71 × 10^{-4}, 3.05 × 10^{-4}/1.62 × 10^{-4}, and 2.30 × 10^{-4}/2.22 × 10^{-4} cm^2 V^{-1} s^{-1}, corresponding to μ_h/μ_e ratios of 4.94, 1.88, and 1.04, respectively. The more balanced μ_h/μ_e ratio of the **PBT1-C : TPTTT-2F** device compared to the other two devices helps to explain the higher FF obtained in the corresponding OSC.

To study their exciton dissociation and charge collection properties, the photocurrent density (J_{ph}) of the OSCs was measured as a function of the effective voltage (V_{eff}). As shown in Fig. 4c, the J_{ph} values reached saturation at a high V_{eff} (>2 V), demonstrating that all the photogenerated excitons were effectively dissociated into free charge carriers and collected by the electrodes. The J_{sat} of the **PBT1-C : TPTTT-2F** device was slightly higher than that of the other two devices, suggesting that the **PBT1-C : TPTTT-2F** device showed improved charge generation and thus enhanced J_{sc}.[45] Under the short circuit conditions, the J_{ph}/J_{sat} ratios of the **PBT1-C : TPT-2F**, **PBT1-C : TPTT-2F**, and **PBT1-C : TPTTT-2F** devices were calculated to be 94.32%, 95.93%, and 96.06%, respectively, suggesting that the **PBT1-C : TPTTT-2F** device had more efficient exciton dissociation and charge collection efficiency than the other two devices.[39]

To study the charge recombination behavior, the dependence of the photocurrent (J_{ph}) on the light intensity (P_{light}) was measured (Fig. 4d). The relationship between J_{sc} and P can be described by the formula $J_{sc} \propto P_{light}^{S}$, where the exponential factor S is an indicator of the extent of bimolecular recombination. As shown in Fig. 4d, the S values of the **PBT1-C : TPT-2F**, **PBT1-C : TPTT-2F**, and **PBT1-C : TPTTT-2F** devices were estimated to be 0.981, 0.990, and 0.999, respectively, suggesting that bimolecular charge recombination was effectively suppressed in all three devices. In particular, the **PBT1-C : TPTTT-2F** device exhibited weaker bimolecular recombination than the other two devices, which could contribute to its higher FF.

The film morphologies of the blend films were investigated by atomic force microscopy (AFM). As shown in Fig. 5, all the blend films showed smooth and uniform surfaces. The root mean square (RMS) roughness of the **PBT1-C : TPTTT-2F** film (1.21 nm) was smaller than those of the **PBT1-C : TPT-2F** (1.46 nm) and **PBT1-C : TPTT-2F** (1.57 nm) films. Moreover, the blend

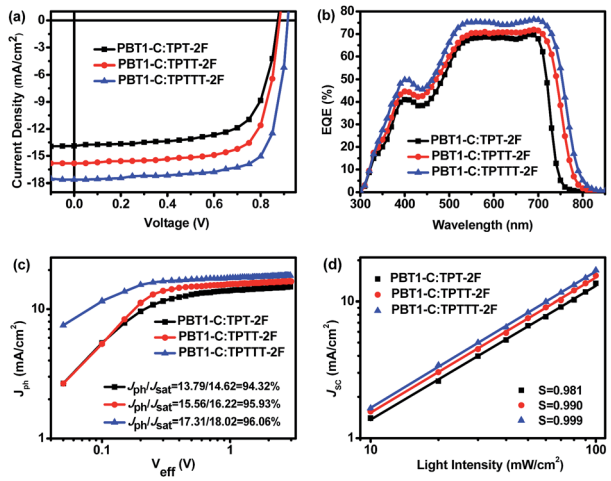

Fig. 4 (a) *J*–*V* curves and (b) EQE spectra of the OSC devices based on the PBT1-C : NFA blend; (c) J_{ph} *versus* V_{eff} plot; and (d) light intensity dependence of J_{sc} of the optimized devices.

Table 2 Summary of the device parameters of the **PBT1-C** : **NFA** blends in solar cells under AM1.5 G Illumination at 100 mW cm^{-2}

NFA	V_{oc} (V)	J_{sc} (mA cm^{-2})	$J_{sc,cal}$ (mA cm^{-2})	FF (%)	PCE[a] (%)
TPT-2F	0.874 (0.871 ± 0.003)	13.89 (13.78 ± 0.09)	13.41	68.6 (66.90 ± 1.52)	8.33 (8.02 ± 0.24)
TPTT-2F	0.881 (0.876 ± 0.007)	15.82 (15.67 ± 0.15)	15.23	73.0 (72.72 ± 0.65)	10.17 (9.98 ± 0.17)
TPTTT-2F	0.916 (0.916 ± 0.002)	17.63 (17.46 ± 0.21)	16.88	74.5 (73.46 ± 0.91)	12.03 (11.78 ± 0.22)

[a] Average values with standard deviations were obtained from 20 devices.

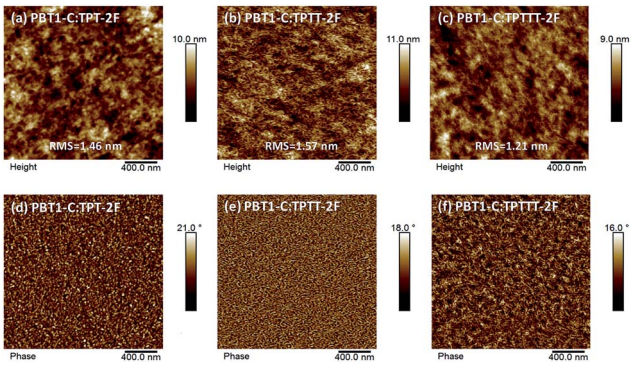

Fig. 5 AFM height images of the blend films (a–c) and the AFM phase images of the blend films (d–f).

films exhibited obvious fibrous features as seen in the AFM phase image, which are favorable for efficient charge transport.

The molecular orientation and their packing structures in both neat and blend films were investigated by grazing incidence wide angle X-ray scattering (GIWAXS) measurements. The 2D diffraction patterns and the corresponding line-cuts are presented in Fig. 6. It can be seen that **TPTT-2F** and **TPTTT-2F** NFAs in neat films adopt a dominant face-on orientation, showing a strong (100) lamellar scattering in the in-plane (IP) direction and a (010) π–π stacking peak in the out-of-plane (OOP) direction. However, in the case of **TPT-2F**, much weaker scatterings were measured, indicating the extended π-conjugation with thienothiophene and cyclopentadithiophene in the

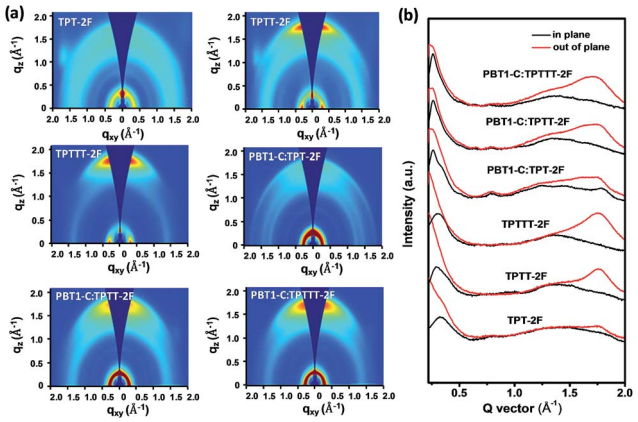

Fig. 6 (a) GIWAXD patterns of **TPT-2F**, **TPTT-2F**, **TPTTT-2F** and their corresponding blends. (b) In-plane (black lines) and out-of-plane (red lines) line-cut profiles of the GIWAXD results.

IDT core of NFA structures increases the intermolecular ordering with enhanced cofacial π–π stacking. The crystal coherence length (CCL) values extracted from the full width at half maximum (FWHM) of the IP (100) peak confirm this trend (28.1 Å for **TPT-2F**, 36.5 Å for **TPTT-2F** and 36.9 Å for **TPTTT-2F**, respectively). With regard to the blend films, a similar trend was measured. A (100) diffraction peak at $q = 0.26$ $Å^{-1}$ appeared, corresponding to the lamellar diffraction of **PBT1-C**. When blended with **PBT1-C**, the OOP (010) diffraction peak of **TPT-2F**, **TPTT-2F** and **TPTTT-2F** is still clear, indicating that they still adopt a predominant face-on orientation in the blend films. Moreover, from **PBT1-C : TPT-2F**, **PBT1-C : TPTT-2F** to **PBT1-C : TPTTT-2F**, the OOP (010) diffraction peak becomes gradually intensified, which is beneficial for charge transport in a vertical direction.

Conclusions

In conclusion, one symmetric non-fullerene acceptor, **TPT-2F**, and two asymmetric non-fullerene acceptors, **TPTT-2F** and **TPTTT-2F**, were synthesized. The influence of the extent of the IDT core conjugation on the electronic properties, charge carrier transport, film morphology, and photovoltaic properties was systematically investigated. From **TPT-2F** to **TPTT-2F** and **TPTTT-2F**, more red-shifted absorption, smaller optical bandgaps, upshifted LUMO energy levels, higher electron mobilities, and stronger intermolecular π–π stacking were obtained. When blended with **PBT1-C**, the V_{oc}, J_{sc}, and FF of the resulting devices improved simultaneously in the order **PBT1-C : TPT-2F** < **PBT1-C : TPTT-2F** < **PBT1-C : TPTTT-2F**. As a result, the **PBT1-C : TPTTT-2F** device achieved a high PCE of 12.03%, which was much higher than that of the **PBT1-C : TPTT-2F** device (10.17%) and the **PBT1-C : TPT-2F** device (8.33%). These results show that extending the conjugation length of the IDT core in A–D–A type non-fullerene acceptors is an effective way to enhance their photovoltaic parameters simultaneously, and thus to achieve high PCEs.

Conflicts of interest

There are no conflicts to declare.

Acknowledgements

This work was financially supported by the National Natural Science Foundation of China (NSFC) (No. 21734001, 51473009, and 21674007). H. Y. W. acknowledges financial

support from the National Research Foundation (NRF) of Korea (2012M3A6A7055540 and 2015M1A2A2057506).

Notes and references

1 S. R. Forrest, *Nature*, 2004, **428**, 911–918.
2 J. Zhao, Y. Li, G. Yang, K. Jiang, H. Lin, H. Ade, W. Ma and H. Yan, *Nat. Energy*, 2016, **1**, 15027.
3 Y. Lin and X. Zhan, *Mater. Horiz.*, 2014, **1**, 470–488.
4 C. B. Nielsen, S. Holliday, H.-Y. Chen, S. J. Cryer and I. McCulloch, *Acc. Chem. Res.*, 2015, **48**, 2803–2812.
5 B. Wang, W. Liu, H. Li, J. Mai, S. Liu, X. Lu, H. Li, M. Shi, C.-Z. Li and H. Chen, *J. Mater. Chem. A*, 2017, **5**, 9396–9401.
6 N. Liang, W. Jiang, J. Hou and Z. Wang, *Mater. Chem. Front.*, 2017, **1**, 1291–1303.
7 J. Hou, O. Inganäs, R. H. Friend and F. Gao, *Nat. Mater.*, 2018, **17**, 119–128.
8 G. Zhang, J. Zhao, P. C. Y. Chow, K. Jiang, J. Zhang, Z. Zhu, J. Zhang, F. Huang and H. Yan, *Chem. Rev.*, 2018, **118**, 3447–3507.
9 H. Zhang, H. Yao, J. Hou, J. Zhu, J. Zhang, W. Li, R. Yu, B. Gao, S. Zhang and J. Hou, *Adv. Mater.*, 2018, **30**, 1800613.
10 Y. Li, J.-D. Lin, X. Che, Y. Qu, F. Liu, L.-S. Liao and S. R. Forrest, *J. Am. Chem. Soc.*, 2017, **139**, 17114–17119.
11 W. Liu, J. Zhang, Z. Zhou, D. Zhang, S. Xu and X. Zhu, *Adv. Mater.*, 2018, **30**, 1800403.
12 Y. Lin, J. Wang, Z. Zhang, H. Bai, Y. Li, D. Zhu and X. Zhan, *Adv. Mater.*, 2015, **27**, 1170–1174.
13 S. Li, Z. Zhang, M. Shi, C.-Z. Li and H. Chen, *Phys. Chem. Chem. Phys.*, 2017, **19**, 3440–3458.
14 W. Chen and Q. Zhang, *J. Mater. Chem. C*, 2017, **5**, 1275–1302.
15 D. He, F. Zhao, L. Jiang and C. Wang, *J. Mater. Chem. A*, 2018, **6**, 8839–8854.
16 C. Li, Y. Xie, B. Fan, G. Han, Y. Yi and Y. Sun, *J. Mater. Chem. C*, 2018, **6**, 4873–4877.
17 N. Qiu, H. Zhang, X. Wan, C. Li, X. Ke, H. Feng, B. Kan, H. Zhang, Q. Zhang, Y. Lu and Y. Chen, *Adv. Mater.*, 2017, **29**, 1604964.
18 W. Zhao, S. Li, H. Yao, S. Zhang, Y. Zhang, B. Yang and J. Hou, *J. Am. Chem. Soc.*, 2017, **139**, 7148–7151.
19 F. Zhao, S. Dai, Y. Wu, Q. Zhang, J. Wang, L. Jiang, Q. Ling, Z. Wei, W. Ma, W. You, C. Wang and X. Zhan, *Adv. Mater.*, 2017, **29**, 1700144.
20 B. Kan, J. Zhang, F. Liu, X. Wan, C. Li, X. Ke, Y. Wang, H. Feng, Y. Zhang, G. Long, R. H. Richard, A. A. Bakulin and Y. Chen, *Adv. Mater.*, 2018, **30**, 1704904.
21 F. Yang, C. Li, W. Lai, A. Zhang, H. Huang and W. Li, *Mater. Chem. Front.*, 2017, **1**, 1389–1395.
22 Y. Li, M. Gu, Z. Pan, B. Zhang, X. Yang, J. Gu and Y. Chen, *J. Mater. Chem. A*, 2017, **5**, 10798–10814.
23 Q. Cao, W. Xiong, H. Chen, G. Cai, G. Wang, L. Zheng and Y. Sun, *J. Mater. Chem. A*, 2017, **5**, 7451–7461.
24 Y. Li, X. Liu, F.-P. Wu, Y. Zhou, Z.-Q. Jiang, B. Song, Y. Xia, Z.-G. Zhang, F. Gao, O. Inganas, Y. Li and L.-S. Liao, *J. Mater. Chem. A*, 2016, **4**, 5890–5897.
25 S. Dai, F. Zhao, Q. Zhang, T.-K. Lau, T. Li, K. Liu, Q. Ling, C. Wang, X. Lu, W. You and X. Zhan, *J. Am. Chem. Soc.*, 2017, **139**, 1336–1343.
26 Y. Li, L. Zhong, F.-P. Wu, Y. Yuan, H.-J. Bin, Z.-Q. Jiang, Z. Zhang, Z.-G. Zhang, Y. Li and L.-S. Liao, *Energy Environ. Sci.*, 2016, **9**, 3429–3435.
27 Y. Yang, Z.-G. Zhang, H. Bin, S. Chen, L. Gao, L. Xue, C. Yang and Y. Li, *J. Am. Chem. Soc.*, 2016, **138**, 15011–15018.
28 Y. Lin, Q. He, F. Zhao, L. Huo, J. Mai, X. Lu, C.-J. Su, T. Li, J. Wang, J. Zhu, Y. Sun, C. Wang and X. Zhan, *J. Am. Chem. Soc.*, 2016, **138**, 2973–2976.
29 X. Liu, B. Xie, C. Duan, Z. Wang, B. Fan, K. Zhang, B. Lin, F. J. M. Colberts, W. Ma, R. A. J. Janssen, F. Huang and Y. Cao, *J. Mater. Chem. A*, 2018, **6**, 395–403.
30 C. Zhang, S. Feng, Y. Liu, R. Hou, Z. Zhang, X. Xu, Y. Wu and Z. Bo, *ACS Appl. Mater. Interfaces*, 2017, **9**, 33906–33912.
31 Y. Nian, Z. Wang, H. Jiang, S. Feng, S. Li, L. Zhang, Y. Cao and J. Chen, *Chin. J. Chem.*, 2018, **36**, 495–501.
32 S. Yu, Y. Chen, L. Yang, P. Ye, J. Wu, J. Yu, S. Zhang, Y. Gao and H. Huang, *J. Mater. Chem. A*, 2017, **5**, 21674–21678.
33 X. Li, T. Yan, H. Bin, G. Han, L. Xue, F. Liu, Y. Yi, Z.-G. Zhang, T. P. Russell and Y. Li, *J. Mater. Chem. A*, 2017, **5**, 22588–22597.
34 L. Feng, Z. Zichun, Z. Cheng, J. Zhang, Q. Hu, T. Vergote, F. Liu, T. P. Russel and X. Zhu, *Adv. Mater.*, 2017, **29**, 1606574.
35 Z. Liang, M. Li, X. Zhang, Q. Wang, Y. Jiang, H. Tian and Y. Geng, *J. Mater. Chem. A*, 2018, **6**, 8059–8067.
36 Y. Liu, Z. Zhang, S. Feng, M. Li, L. Wu, R. Hou, X. Xu, X. Chen and Z. Bo, *J. Am. Chem. Soc.*, 2017, **139**, 3356–3359.
37 W. Gao, M. Zhang, T. Liu, R. Ming, Q. An, K. Wu, D. Xie, Z. Luo, C. Zhong, F. Liu, F. Zhang, H. Ye and C. Yang, *Adv. Mater.*, 2018, **30**, 1800052.
38 W. Zhai, A. Tang, B. Xiao, X. Wang, F. Chen and E. Zhou, *Sci. Bull.*, 2018, **63**, 845–852.
39 S. Dai, T. Li, W. Wang, Y. Xiao, T. K. Lau, Z. Li, K. Liu, X. Lu and X. Zhan, *Adv. Mater.*, 2018, **30**, 1706571.
40 J. Zhu, Y. Wu, J. Rech, J. Wang, K. Liu, T. Li, Y. Lin, W. Ma, W. You and X. Zhan, *J. Mater. Chem. C*, 2018, **6**, 66–71.
41 J. Zhu, Z. Ke, Q. Zhang, J. Wang, S. Dai, Y. Wu, Y. Xu, Y. Lin, W. Ma, W. You and X. Zhan, *Adv. Mater.*, 2018, **30**, 1704713.
42 Z. Kang, S.-C. Chen, Y. Ma, J. Wang and Q. Zheng, *ACS Appl. Mater. Interfaces*, 2017, **9**, 24771–24777.
43 Y. Li, K. Yao, H. Yip, F. Ding, Y. Xu, X. Li, Y. Chen and K. Y. Alex, *Adv. Funct. Mater.*, 2014, **24**, 3631–3638.
44 T. Liu, L. Huo, C. Sreelakshmi, C. Kai, G. Han, Q. Feng, M. Xiangyi, D. Xie, M. Wei, Y. Yi, J. M. Hodgkiss, L. Feng, W. Jing, C. Yang and Y. Sun, *Adv. Mater.*, 2018, **30**, 1707353.
45 W. Wang, C. Yan, T. K. Lau, J. Wang, K. Liu, Y. Fan, X. Lu and X. Zhan, *Adv. Mater.*, 2017, **29**, 1701308.

